A&A 440, 111–120 (2005)
DOI: 10.1051/0004-6361:20052982

Astronomy & Astrophysics

Integrated spectral analysis of 18 concentrated star clusters in the Small Magellanic Cloud⋆,⋆⋆

A. E. Piatti[1], J. F. C. Santos Jr.[2], J. J. Clariá[3], E. Bica[4], A. V. Ahumada[3], and M. C. Parisi[3]

[1] Instituto de Astronomía y Física del Espacio, CC 67, Suc. 28, 1428 Buenos Aires, Argentina
[2] Departamento de Física, ICEx, UFMG, CP 702, 30123-970 Belo Horizonte, MG, Brazil
e-mail: jsantos@fisica.ufmg.br
[3] Observatorio Astronómico, Laprida 854, 5000 Córdoba, Argentina
[4] Depto. de Astronomia, UFRGS, CP 15051, 91500-970 Porto Alegre, Brazil

Received 3 March 2005 / Accepted 18 May 2005

Abstract. We present in this study flux-calibrated integrated spectra in the range (3600–6800) Å for 18 concentrated SMC clusters. Cluster reddening values were estimated by interpolation between the extinction maps of Burstein & Heiles (1982, AJ, 87, 1165) and Schlegel et al. (1998, ApJ, 500, 525). The cluster parameters were derived from the template matching procedure by comparing the line strengths and continuum distribution of the cluster spectra with those of template cluster spectra with known parameters and from the equivalent width (*EW*) method. In this case, new calibrations were used together with diagnostic diagrams involving the sum of *EW*s of selected spectral lines. A very good agreement between ages derived from both methods was found. The final cluster ages obtained from the weighted average of values taken from the literature and the present measured ones range from 15 Mr (e.g. L 51) to 7 Gyr (K 3). Metal abundances have been derived for only 5 clusters from the present sample, while metallicity values directly averaged from published values for other 4 clusters have been adopted. Combining the present cluster sample with 19 additional SMC clusters whose ages and metal abundances were put onto a homogeneous scale, we analyse the age and metallicity distributions in order to explore the SMC star formation history and its spatial extent. By considering the distances of the clusters from the SMC centre instead of their projections onto the right ascension and declination axes, the present age-position relation suggests that the SMC inner disk could have been related to a cluster formation episode which reached the peak ∼2.5 Gyr ago. Evidence for an age gradient in the inner SMC disk is also presented.

Key words. galaxies: star clusters – techniques: spectroscopic – Magellanic Clouds

1. Introduction

The Small Magellanic Cloud (SMC) is a galaxy rich in star clusters of all ages and different types of field populations (Hodge 1988, 1989; Dolphin et al. 2001). An interesting feature in the chemical enrichment history of the SMC known up to now is that no very metal-poor old cluster has been observed in this galaxy (Da Costa 1991; Dutra et al. 2001). Piatti et al. (2001) studied 5 outlying intermediate-age clusters in the SMC and, combined to other data in the literature, studied the age-metallicity relationship, showing that epochs of sudden chemical enrichment take place in the age-metallicity plane. This favours a bursting star formation history for the SMC as opposed to a continuous one. Recently, Piatti et al. (2005) confirmed, with new observations, the occurrence of an important bursting star formation episode at ∼2.5 Gyr.

A star cluster spectral library at the SMC metallicity level can be useful for analyses of star clusters in dwarf galaxies observable by means of ground-based large telescopes as well as the Hubble Space Telescope (HST). In addition, such metal-poor library appears to be also useful for the study of a fraction of star clusters in massive galaxies, due to cannibalism. Indeed, in the Milky Way galaxy at least four globular clusters have been accreted from the Sagittarius dwarf galaxy (Da Costa & Armandroff 1995), and the open clusters AM-2 and Tombaugh 5 appear to be related to the Canis Major dwarf galaxy (Bellazzini et al. 2004).

In this sense, spectral libraries of stars (e.g., Silva & Cornell 1992), open clusters (Piatti et al. 2002a) or star clusters in general (Bica & Alloin 1986) are important datasets for spectral classifications and extraction of parameter information for target stars or star clusters (e.g., Piatti et al. 2002b) and galaxies (e.g., Bica 1988).

Samples of integrated spectra of SMC clusters were initially small, corresponding to the most prominent clusters such as NGC 121, NGC 419, NGC 330 and others (Bica & Alloin 1986; Santos et al. 1995). Ahumada et al. (2002) analysed

⋆ FITS spectra are only available in electronic form at the CDS via anonymous ftp to cdsarc.u-strasbg.fr (130.79.128.5) or via http://cdsweb.u-strasbg.fr/cgi-bin/qcat?J/A+A/440/111
⋆⋆ Figures 1 to 18 are only available in electronic form at http://www.edpsciences.org

integrated spectra in the range 3600–6800 Å for 16 star clusters in the SMC, estimating ages and reddening values. That study has constituted a fundamental step forward towards a cluster spectral library at low metallicities.

A comprehensive catalogue of SMC clusters was produced by Bica & Schmitt (1995), and updated in Bica & Dutra (2000). In it, cross-identifications for different designations, coordinates, angular sizes and references to previous catalogues are provided. The angular distribution of SMC clusters has been discussed in Bica & Schmitt (1995): most clusters are projected on the SMC main body and a significant fraction are outlyers. The line-of-sight (LOS) depth of populous clusters in the SMC was analysed by Crowl et al. (2001), who found significant depth effects, with a triaxial shape of 1:2:4 for the declination, the right ascension, and the LOS depth of the SMC, respectively.

The present cluster sample complements previous ones, in an effort to provide a spectral library with several clusters per age bin. At the same time, we study the clusters themselves individually, determining their parameters and analysing the age distribution, in order to explore the SMC star formation history and its spatial extent. To estimate the clusters' ages, we employ the new calibrations and diagnostic diagrams recently provided by Santos & Piatti (2004, hereafter SP) for visible integrated spectra, along with template spectra (e.g., Santos et al. 1995; Ahumada et al. 2002). We confirm the reliability of the procedure proposed by SP in determining clusters' ages, since we included in the sample not only unstudied or poorly studied clusters but also some control clusters with well-known fundamental parameters.

In Sect. 2 we describe the different sets of observations and the reduction procedure performed. The analyses of the integrated spectra through the template matching and equivalent width methods are developed in Sect. 3, in which we also include some considerations for individual clusters. In Sect. 4 we discuss the present results in the light of the star formation history of the SMC. Finally, in Sect. 5 we summarize the main conclusions of this work.

2. Spectra acquisition and reduction

The objects studied here are part of a systematic spectroscopic survey of SMC star clusters which is being undertaken at Complejo Astronómico El Leoncito (CASLEO) in San Juan (Argentina) and Cerro Tololo Inter-American Observatory (CTIO, Chile). The first results of this survey dealt with 16 concentrated star clusters (Ahumada et al. 2002), approximately half of which constitute previously unstudied objects.

The observations analysed in this study were carried out with the CASLEO 2.15 m telescope during four nights in November 2001 and five nights in October 2002 and with the CTIO 1.5 m telescope during four nights in September 2003. In all the CASLEO runs we empoyed a CCD camera containing a Tektroniks chip of 1024×1024 pixels attached to a REOSC spectrograph (simple mode), the size of each pixel being $24\ \mu\text{m} \times 24\ \mu\text{m}$; one pixel corresponds to $0.94''$ on the sky. The slit was set in the East-West direction and the observations were performed by scanning the slit across the objects in the North-South direction in order to get a proper sampling of cluster stars. The long slit corresponding to $4.7'$ on the sky, allowed us to sample regions of the background sky. We used a grating of 300 grooves mm^{-1}, producing an average dispersion in the observed region of ≈140 Å/mm (3.46 Å/pixel). The spectral coverage was ≈3600–6800 Å. The seeing during the CASLEO nights was typically $2.0''$. The slit width was $4.2''$, providing a resolution [full width at half-maximum (*FWHM*)] of ≈14 Å, as deduced from the comparison lamp lines. For the CTIO observations, we used a CCD Loral 1K chip of 1200×800 pixels (pixel diameter = 15 μm), controlled by the CTIO ARCON 3.9 data acquisition system at a gain of 2.05 e^- ADU^{-1} with a readout noise of 7.4 e^- ADU^{-1}. The same slit width of $4.2''$ as in CASLEO was used at CTIO, thus providing a resolution of about 11 Å. The seeing during the CTIO observations was typically $1.0''$. At least two exposures of 30 min of each object were taken in order to correct for cosmic rays. Standard stars from the list of Stone & Baldwin (1983) were also observed at both observatories for flux calibrations. Bias, darks, dome and twilight sky and tungsten lamp flats were taken and employed in the reductions.

The reduction of the spectra was carried out with the IRAF[1] package at the Observatorio Astronómico de Córdoba (Argentina – CASLEO data) and at the Instituto de Astronomía y Física del Espacio (Argentina – CTIO data) following the standard procedures. Summing up, we subtracted the bias and used flat-field frames- previously combined – to correct the frames for high and low spatial frequency variations. We also checked the instrumental signature with the acquisition of dark frames. Then, we performed the background sky subtraction using pixel rows from the same frame, after having cleaned the background sky regions from cosmic rays. We controlled that no significant background sky residuals were present on the resulting spectra. The cluster spectra were extracted along the slit according to the cluster size and available flux. Five of these clusters (K 5, K 7, NGC 269, K 28 and NGC 411) have one very bright star located close to their main bodies. The spectra were then wavelength calibrated by fitting observed He-Ne-Cu (CASLEO) or He-Ar (CTIO) comparison lamp spectra with template spectra. The rms errors involved in these calibrations are in average 0.40 Å for both observatories. Finally, we applied to the cluster spectra extinction corrections and flux calibrations derived from the observed standard stars. We decided to use the sensitivity function derived from all the standard stars observed each night. This calibrated function turned out to be nearly the same as the nightly sensitivity functions, but more robustly defined and with a smaller rms error. In addition, cosmic rays on the cluster spectra were eliminated. Table 1 presents the cluster sample including the averaged signal-to-noise (S/N) ratios of the spectra.

[1] IRAF is distributed by the National Optical Astronomy Observatories, which is operated by the Association of Universities for Research in Astronomy, Inc., under contract with the National Science Foundation.

Table 1. The sample clusters.

Name[a]	α_{2000} (h:m:s)	δ_{2000} (°:′:″)	D (′)	Origin	S/N
L 5, ESO 28-SC 16	0:22:40	–75:04:29	1.10	CTIO	20
K 5, L 7, ESO 28-SC 18	0:24:43	–73:45:18	1.80	CTIO	30
K 3, L 8, ESO 28-SC 19	0:24:47	–72:47:39	3.40	CTIO	30
K 6, L 9, ESO 28-SC 20	0:25:26	–74:04:33	1.00	CTIO	35
K 7, L 11, ESO 28-SC 22	0:27:46	–72:46:55	1.70	CTIO	30
HW 8	0:33:46	–73:37:59	1.70	CASLEO	20
NGC 269, K 26, L 37, ESO 29-SC 16	0:48:21	–73:31:49	1.20	CASLEO	30
L 39, SMC_OGLE 54	0:49:18	–73:22:20	0.70	CASLEO	35
K 28, L 43, ESO 51-SC 4	0:51:42	–71:59:52	1.70	CTIO	15
NGC 294, L 47, ESO 29-SC 22, SMC_OGLE 90	0:53:06	–73:22:49	1.70	CASLEO	45
L 51, ESO 51-SC 7	0:54:54	–72:06:46	1.00	CASLEO	50
K 42, L 63, SMC_OGLE 124	1:00:34	–72:21:56	0.85	CASLEO	40
L 66, SMC_OGLE 129	1:01:45	–72:33:52	1.10	CASLEO	100
NGC 411, K 60, L 82, ESO 51-SC 19	1:07:55	–71:46:08	2.10	CTIO	55
NGC 419, K 58, L 85, ESO 29-SC 33, SMC_OGLE 159	1:08:19	–72:53:03	2.80	CASLEO	70
NGC 422, K 62, L 87, ESO 51-SC 22	1:09:25	–71:46:00	1.00	CASLEO	30
IC 1641, HW 62, ESO 51-SC 21	1:09:39	–71:46:07	0.75	CASLEO	45
NGC 458, K 69, L 96, ESO 51-SC 26	1:14:52	–71:33:00	2.60	CASLEO	45

[a] Cluster identifications are from Kron (1956, K), Lindsay (1958, L), Hodge & Wright (1974, HW), Lauberts (1982, ESO), Pietrzyński et al. (1998, SMC_OGLE).

3. Analysis of the cluster spectra

The cluster parameters were derived by means of two methods: the template matching method, in which the observed spectra are compared and matched to template spectra with well-determined properties (e.g. Piatti et al. 2002a, and references therein), and the equivalent width (*EW*) method, in which diagnostic diagrams involving the sum of *EW*s of selected spectral lines were employed together with their calibrations with age and metallicity (SP). In the first method, a high weight is assigned to the matching of the overall continuum, while in the second method the spectral lines are the observables that define cluster parameters. Both methods rely on the library of star cluster integrated spectra with well-determined properties, accomplished in various studies (e.g. Bica & Alloin 1986; Piatti et al. 2002a, and references therein) and made available through the CDS/Vizier catalogue database at `http://vizier.u-strasbg.fr/cgi-bin/VizieR?-source=III/219` (Santos et al. 2002).

3.1. Template matching method

All 18 clusters in our sample are well represented by a wide variety of stellar populations, as may be noticed from their spectra overall appearance. The template spectra useful for the present sample are: Yb (5–10 Myr), Yd (40 Myr), Ye (45–75 Myr), Yg (200–350 Myr), Yh (0.5 Gyr), Ia (1 Gyr) and Ib (3–4 Gyr), which represent young and intermediate-age populations built from Galactic open clusters (Piatti et al. 2002a), and G3 (>10 Gyr, [Fe/H] = –1.0), G4 (>10 Gyr, [Fe/H] = –1.5) and G5 (>10 Gyr, [Fe/H] = –2.0), which represent old stellar populations built from Galactic globular clusters (Bica 1988).

The template matching method consists of achieving the best possible match between the analysed cluster spectrum and a template spectrum of known age and metallicity. In this process we selected, among the available template spectra, the ones which minimize the flux residuals, calculated as the difference (cluster – template)/cluster. Note that differences between the cluster and template spectra are expected to be found due to variations in the stellar composition of the cluster, such as the presence of a relatively bright star with particular spectral features or contamination of a field star close to the direction towards the cluster.

Since the continuum distribution is also affected by reddening, we first adopted a colour excess $E(B-V)$ for each cluster, taking into account the Burstein & Heiles (1982, hereafter BH) and Schlegel et al. (1998, hereafter SFD) extinction maps, and then corrected the observed spectra accordingly before applying the template match method. We recall that one can deredden an integrated spectrum and simultaneously estimate the cluster age. However, in order to make the age estimate more robust, we preferred to match reddening corrected cluster spectra with template spectra. Thus, instead of having to handle two variables in the match (reddening and age), we limit it to find only the cluster age.

The maps of BH and SFD are frequently used to estimate the colour excesses of clusters located in the direction towards the Magellanic Clouds (see, e.g., Piatti et al. 2001; Dutra et al. 2001). SFD found that at high-latitude regions, their dust maps correlate well with maps of H I emission, but deviations are coherent in the sky and are especially conspicuous in regions of saturation of HI emission towards denser clouds and of formation of H_2 in molecular clouds. The SMC is quite transparent, the average foreground and internal reddenings being 0.01 and 0.04, respectively (Dutra et al. 2001). The typical

Table 2. Equivalent widths (Å).

Feature	K Ca II	H_δ	*G* band (CH)	H_γ	H_β	Mg I	S_h	S_m
Windows (Å)	3908–3952	4082–4124	4284–4318	4318–4364	4846–4884	5156–5196		
Cluster								
L 5	5.2	7.3	5.1	8.8	7.2	4.0	23.3	14.3
K 5	6.9	8.5	5.1	9.7	6.3	3.5	24.5	15.5
K 3	6.8	5.4	6.2	3.9	4.5	3.4	13.9	16.5
K 28	9.1	2.9	4.1	3.4	2.9	3.4	9.3	16.6
K 6	5.5	8.2	4.7	6.6	4.6	4.0	19.4	14.3
K 7	10.4	2.5	7.0	4.7	4.6	4.0	11.8	21.4
HW 8	4.4	7.9	1.3	6.3	6.3	3.2	20.4	8.9
NGC 269[a]	4.7	11.9	3.3	9.6	–	4.0	–	11.9
L 39	2.3	3.1	1.3	3.1	2.2	0.7	8.4	4.2
K 28	9.1	2.9	4.1	3.4	2.9	3.4	9.3	16.6
NGC 294	4.1	10.3	2.1	11.2	7.0	1.7	28.5	7.8
L 51	1.0	7.6	0.6	4.3	4.9	1.2	16.8	2.7
K 42	1.2	4.5	1.1	4.8	4.2	0.5	13.4	2.8
L 66	0.6	5.8	-0.3	2.7	3.8	1.0	12.3	1.2
NGC 411	6.5	8.7	5.3	8.9	6.0	2.7	23.6	14.5
NGC 419	6.9	8.2	3.5	7.7	7.1	1.9	22.9	12.3
NGC 422	2.1	8.2	1.3	6.2	6.1	1.2	20.5	4.6
IC 1641	4.0	9.6	2.3	8.1	6.2	1.5	23.9	7.7
NGC 458	1.9	8.6	0.8	8.3	7.9	2.1	24.8	4.8

[a] The spectrum of the symbiotic nova SMC 3 was subtracted from the observed spectrum.

reddening towards the SMC estimated from the median dust emission in annuli surrounding the galaxy is $E(B-V) = 0.037$ (SFD). Therefore, we assume that relatively high SFD values are saturated and we then use the BH values. For clusters with non saturated SFD values, the difference between SFD and BH colour excesses resulted in, at the most, 0.02 mag; the SFD zero-point being made consistent with the BH maps by subtracting 0.02 mag in $E(B-V)_{\rm SFD}$. The results are shown in Figs. 1 to 18.

3.2. Equivalent width method

Before measuring *EW*s in the observed spectra, they were set to the rest-frame according to the Doppler shift of H Balmer lines. Next, the spectra were normalized to $F_\lambda = 1$ at 5870 Å and smoothed to the typical resolution of the database (≈10–15 Å).

Spectral fluxes at 3860, 4020, 4150, 4570, 4834, 4914 and 6630 Å were used as guidelines in order to define the continuum according to Bica & Alloin (1986). The *EW*s of H Balmer, K Ca II, G band (CH) and Mg I (5167 + 5173 + 5184 Å) were measured within the spectral windows defined by Bica & Alloin (1986) and using IRAF task *splot*. Boundaries for the K Ca II, G band (CH), Mg I, Hδ, Hγ and Hβ spectral windows are, respectively, (3908–3952) Å, (4284–4318) Å, (5156–5196) Å, (4082–4124) Å, (4318–4364) Å, and (4846–4884) Å. Such a procedure has been applied consistently making the *EW*s from integrated spectra safely comparable with the well-known cluster database. Table 2 presents these measurements as well as the sum of *EW*s of the three metallic lines (S_m) and of the three Balmer lines H_δ, H_γ and H_β (S_h). S_m and S_h are shown to be useful in the discrimination of old, intermediate-age and young systems (Rabin 1982; Dutra et al. 1999, SP). Typical errors of ≈10% on individual *EW* measurements were obtained by tracing slightly different continua. By using the sums of *EW*s S_h and S_m separately, the *EW* relative errors are lowered (≈7% smaller range than the individual *EW* errors), improving their sensitivity to cluster age and metallicity (SP).

The sums of *EW*s S_h and S_m presented in Table 2 were used to estimate cluster parameters according to their calibrations as a function of age and metallicity given by SP. Such calibrations are based on visible integrated spectra of Galactic and Magellanic Cloud clusters for which age and metallicity were well-determined and put within homogeneous scales. In summary, the calibrations, aided by diagnostic diagrams involving S_m and S_h, allow one to obtain age for star clusters younger than ≈10 Gyr and metallicity for older ones. Yet, a degeneracy occurs for globular age-like clusters with [Fe/H] > −1.4 and intermediate-age clusters ($2.5 < t$(Gyr) < 10), which cannot be discriminated using this method. In this case, it is necessary to constrain age by using an independent method (e.g., the template matching one) and then obtain metallicity with the SP's calibration, if the cluster is old. It is worth mentioning that only 5 SMC clusters are included in the SP's calibration, but since they follow the general trend of Galactic clusters in the diagnostic diagrams, we judged safe to apply that calibration to the present sample. The derived ages and metallicities for the cluster sample are summarized in Table 3. In Cols. 6 and 9, the methods used to obtain age and metallicity are indicated. Except for K 28, with a low S/N spectrum, all remaining clusters were age-ranked according to the *EW* method based on S_h and S_m measurements. In the case of NGC 269, we decided to use only S_m, since the substraction of the spectrum of the symbiotic nova SMC 3 could affect the *EW*s of the cluster H Balmer lines (see details in Sect. 3.3.7). The template method was applied to the whole sample either independently from the

Table 3. Cluster parameters.

Cluster	$E(B-V)$	$t_{\rm literature}$ (Gyr)	Ref.	$t_{\rm m}$ (Gyr)	method	$t_{\rm adopted}$ (Gyr)	[Fe/H]	Ref.
L 5	0.03	4.1	1	0.8	$S_{\rm h}, S_{\rm m}$ – template	3.0 ± 1.5	-1.1 ± 0.2	1, 9
K 5	0.02	2.0	1	0.8	$S_{\rm h}, S_{\rm m}$ – template	1.2 ± 0.5	-0.5 ± 0.2	1, 9
K 3	0.02	7.0 ± 1.0	2, 4	7.0	$S_{\rm h}, S_{\rm m}$ + template	7.0 ± 1.0	-1.20 ± 0.2	2, 9
K 6	0.03	1.3	7	2.0	$S_{\rm h}, S_{\rm m}$ + template	1.6 ± 0.4	–0.7	9
K 7	0.02	3.5	3	4.0	$S_{\rm h}, S_{\rm m}$ + template	3.5 ± 0.5	–1.0	3
HW 8	0.03			0.05	$S_{\rm h}, S_{\rm m}$ – template	0.05 ± 0.02		
NGC 269	0.01			0.6	$S_{\rm m}$ – template	0.6 ± 0.2		
L 39	0.01			0.015	$S_{\rm h}, S_{\rm m}$ – template	0.015 ± 0.010		
K 28	0.06	2.1	2	1.0	template	1.5 ± 0.6	-1.0 ± 0.2	2, 9
NGC 294	0.02			0.3	$S_{\rm h}, S_{\rm m}$ – template	0.3 ± 0.1		
L 51	0.07			0.015	$S_{\rm h}, S_{\rm m}$ – template	0.015 ± 0.010		
K 42	0.06			0.045	$S_{\rm h}, S_{\rm m}$ – template	0.045 ± 0.015		
L 66	0.06			0.015	$S_{\rm h}, S_{\rm m}$ – template	0.015 ± 0.010		
NGC 411	0.03	1.5 ± 0.2	2, 6, 8	1.0	$S_{\rm h}, S_{\rm m}$ – template	1.5 ± 0.3	-0.7 ± 0.2	2, 6, 8
NGC 419	0.03	1.6 ± 0.4	2, 4	0.8	$S_{\rm h}, S_{\rm m}$ – template	1.2 ± 0.4	–0.7	2
NGC 422	0.03			0.3	$S_{\rm h}, S_{\rm m}$ – template	0.3 ± 0.1		
IC 1641	0.03			0.3	$S_{\rm h}, S_{\rm m}$ – template	0.3 ± 0.1		
NGC 458	0.02	0.17 ± 0.03	2, 5	0.05	$S_{\rm h}, S_{\rm m}$ – template	0.13 ± 0.06	–0.23	2

References: (1) Piatti et al. (2005); (2) Piatti et al. (2002b); (3) Mould et al. (1992); (4) Rich et al. (2000); (5) Alcaino et al. (2003); (6) Alves & Sarajedini (1999); (7) Matteucci et al. (2002); (8) Leonardi & Rose (2003); (9) this work.

EW method (minus sign in Col. 6) or in conjunction with the *EW* method (plus sign in Col. 6). Note that we only had to employ template and *EW*s methods in conjunction for clusters in the age-metallicity degeneracy range. We found a very good agreement between ages derived from both methods. The final cluster ages obtained from the weighted average of values taken from the literature (Cols. 3 and 4) and the measured present ones ($t_{\rm m}$) are listed in Col. 7. Their respective errors take into account the dispersion of the values averaged and/or the estimated uncertainties for $t_{\rm m}$. Column 2 lists the colour excesses adopted for the clusters.

The last two columns of Table 3 show the cluster metallicities adopted whenever possible and their corresponding sources, respectively. Some clusters have metal abundances directly averaged from published values. For K 3, we used Eq. (8) of SP. Three clusters (L 5, K 5 and K 28) have metallicities derived from a technique involving morphological features in the cluster colour-magnitude diagram (CMD) (Piatti et al. 2002b, 2005), which we corrected for age degeneracy using the present ages. Finally, we fitted Padova isochrones (Girardi et al. 2002) to the K 6 CMD obtained by Matteucci et al. (2002) and yielded a cluster metallicity of [Fe/H] = −0.7, assuming for the cluster the reddening and age of Table 3 and the SMC apparent distance modulus $(m-M) = 19.0$ (Cioni et al 2000). The fit was performed on an extracted CMD containing stars distributed around 2′ from the cluster centre, with the aim of avoiding field star contamination.

3.3. Individual cluster analysis

We have revised the literature on the cluster parameters below. More weight has been assigned to ages determined from isochrone fitting to CMD data, but when such information was not available, ages based on integrated indices were also considered. No previous age information was found either for HW 8 (Fig. 6) or IC 1641 (Fig. 17).

3.3.1. L 5

Piatti et al. (2005) have derived $t = 4.3$ Gyr and [Fe/H] = −1.2 for this cluster. Much like K 5, the age of L 5 has been estimated to be 0.8 Gyr according to both methods employed in the present work. A correction to the metallicity provided by Piatti et al. (2005) revised it to [Fe/H] = −1.1 for its significantly younger age. Figure 1 shows the best template combination for L 5, i.e., the average of Ia and Yh templates with a reddening of $E(B-V) = 0.03$. This is the cluster with the most discrepant age in the sample with respect to the published cluster ages. We did not find any reason for such difference, apart from a relative low S/N ratio in the observed spectrum.

3.3.2. K 5

Bica et al. (1986) derived for K 5 the following parameters from integrated photometry of the Hβ and G band absorption features: $[Z/Z_{\odot}] = -1.1 \pm 0.2$ and $t = 3.2 \pm 0.3$ Gyr, while the recent study by Piatti et al. (2005) yields [Fe/H] = −0.6 and $t = 2.0$ Gyr. The template method estimate for K 5 age is $t = 0.8$ Gyr, according to its spectral resemblance to an average of templates Ia and Yh, after applying a reddening correction of $E(B-V) = 0.02$ (Fig. 2). Its metallicity has been corrected to [Fe/H] = −0.5, following an age revision on the Piatti et al. (2005) value.

3.3.3. K 3

Rich et al. (1984) determined an age of 5–8 Gyr from BR photometry and isochrone fitting. K 3 was included in the integrated photometric study by Bica et al. (1986), who derived $t \geq 10$ Gyr and $[Z/Z_{\odot}] = -1.5 \pm 0.2$. Mighell et al. (1998) obtained [Fe/H] $= -1.16 \pm 0.09$, $t = 6.0 \pm 1.3$ Gyr and $E(B-V) = 0.0$ from HST observations and morphological parameters defined in the CMD. More recently, Brocato et al. (2001) presented a HST CMD of K 3 making available its photometry, on which we have superimposed Padova isochrones (Girardi et al. 2002) to obtain essentially the same parameters as those derived by Mighell et al. (1998). In the present study, an intermediate age for K 3 is confirmed, being this the oldest cluster in the present sample. The template matching method gives for this cluster ≈7 Gyr as a result of averaging the G3 and Ia templates (Fig. 3). Both age and metallicity obtained in the present analysis show good agreement with results from previous studies.

3.3.4. K 6

From CCD BV photometry selected for an inner region ($r < 35''$) of K 6, Matteucci et al. (2002) derived an age of 1–1.3 Gyr for this cluster. The spectrum comparison leads to a match of K 6 spectrum with the template Ib (3–4 Gyr), combined with a reddening correction of $E(B-V) = 0.03$ (Fig. 4). However, a smaller age is suggested by the EW method, being $t = 1.6$ Gyr the final adopted value. By fitting Padova isochrones (Girardi et al. 2002) to the CMD data of Matteucci et al. (2002) and assuming the above mentioned age and the apparent distance modulus $(m-M) = 19$ (Cioni et al 2000), an estimate of the cluster metallicity was also obtained, i.e., [Fe/H] $= -0.7$.

3.3.5. K 7

Mould et al. (1992) carried out CCD BR photometry of K 7 obtaining $t = 3.5 \pm 1$ Gyr by isochrone fitting with $E(B-V) = 0.04$. The template spectrum Ib (3–4 Gyr) was initially tried as a match to the K 7 spectrum, but its redder colour cannot be accounted for by a large reddening correction exclusively. Mould et al. (1992) pointed out the presence of two carbon stars close to the cluster centre, which are the probable contributors to the red appearance of its integrated spectrum. In order to check whether this is the case, a combination of the Ib spectrum with a carbon star spectrum taken from Barnbaum et al. (1996) spectral library was tried. Specifically, the spectrum of the nearly solar metallicity carbon star BM Gem (Abia & Isern 2000) was used in the analysis. According to our observations, in the cluster spatial profile the presence of the bright star stands out over the bulk of the cluster light. We then extracted the integrated spectrum of the cluster plus the carbon star and of the carbon star spectrum alone. The flux ratio at 5870 Å between the carbon star spectrum and the integrated one turned out to be 0.35. As a matter of fact, there is a good match to K 7 spectrum if the template Ib is combined with the carbon star in a proportion of 65% and 35% of the total light at 5870 Å, respectively, and the resulting spectrum is reddening corrected by $E(B-V) = 0.02$ (Fig. 5). Relatively large residual spectral differences still remain between the spectra, which may be attributed to the higher metallicity of the carbon star employed as template. No metallicity has been estimated for this cluster.

3.3.6. NGC 269

This is an interesting case in which there is a bright emission line star contributing significantly to the cluster integrated spectrum. Such a situation, which we had found in previous cluster observations (e.g. Santos et al. 1995), has been successfully treated by subtracting the star spectrum from the total integrated one, leaving a spectrum which better represents the cluster average population. Although such a procedure introduced noise in the resulting spectrum, it allowed us to estimate the cluster age using the template matching method. The bright star in NGC 269 spectrum is SMC 3, a symbiotic nova composed by a M0 giant and a white dwarf orbiting each other in a period of ≈4 years (Kahabka 2004). Its spectrum was published in the spectrophotometric atlas of Munari & Zwitter (2002). The OGLE database includes a CMD for this cluster (OGLE-CL-SMC0046), although an age estimate was not provided there (Pietrzynski et al. 1998; Pietrzynski & Udalski 1999). This CMD shows that SMC 3 is ≈2 mag brighter in V than the next bright star in the cluster. In detail, the procedure adopted was to subtract the total integrated spectrum from a scaled SMC 3 spectrum by assuming that all the emission present in the integrated spectrum is due to SMC 3. In this manner, the difference between the spectra which minimizes the emission line residuals was obtained when the star contributes with 60% of the total flux at 5870 Å. Since the spectra were observed at different epochs and SMC 3 is variable, the small but clearly visible residuals reflect such irregularities. Another point that allows one to check the reliability of this procedure is the fact that absorption molecular bands present in SMC 3 spectrum almost disappear in the resulting spectrum. The subtracted spectrum was then submitted to the template matching method (Fig. 7), being similar to an average of the templates Yh and Ia (750 Myr). Such an age is in agreement with the clusters SWB type III-IV (Searle et al. 1980). González et al. (2004) have assigned an age of 500 Myr to NGC 269, based on the integrated colour parameterization ("s" parameter) by Elson & Fall (1988). However, it should be kept in mind that González et al. (2004) age ranking is intended to group clusters of similar integrated properties and their age groups encompass wide age ranges.

3.3.7. L 39

The OGLE database includes a CMD for this cluster (OGLE-CL-SMC0054), with an isochrone based age estimate of 100 ± 23 Myr (Pietrzynski et al. 1998; Pietrzynski & Udalski 1999). A new age estimate based both on a different areal extraction of the same data and on the same isochrones revises it down to 80 ± 20 Myr (de Oliveira et al. 2000). According to González et al. (2004), L 39 is similar to 50 Myr old clusters. We have

found that the cluster is 15 ± 10 Myr old, its steep continuum resembling those of L 51 and L 66 (Fig. 8).

3.3.8. K 28

Piatti et al. (2001) obtained CCD Washington photometry for this cluster deriving [Fe/H] = −1.45 ± 0.13 and t = 2.1 ± 0.5 Gyr, with a reddening within the range $0.06 < E(B-V) < 0.16$. In the present analysis, we have not applied the *EW* method to derive parameters for K 28 because its integrated spectrum has low S/N ratio, although it still seems to be adequate to the template matching method. Indeed, using the latter, we have got a good match for the template Ia (1 Gyr) combined with a reddening of $E(B-V) = 0.06$ (Fig. 9). By revising down the age obtained by Piatti et al. (2001), a corrected metallicity of [Fe/H] = −1.0 was derived.

3.3.9. NGC 294

This cluster (OGLE-CL-SMC0090) has a CMD included in the OGLE database. Its estimated age based on the isochrone fitting method is 316 ± 73 Myr (Pietrzynski et al. 1998; Pietrzynski & Udalski 1999). The study published by de Oliveira et al. (2000) gives 300 ± 50 Myr. Since there is no SWB type assigned to this cluster, González et al. (2004) included NGC 294 in their 1 Gyr cluster group due to the similarity of its integrated colours to the colours of SWB IV clusters. This age seems to be in disagreement with the previously mentioned works and also with ours, which gives $t = 300 \pm 100$ Myr (Fig. 10). Visible cluster images do not show any bright star in the cluster core, and therefore the age discrepancy cannot be due to sampling effects.

3.3.10. L 51

This cluster has spectral similarities with L 66, for which a CMD is available (see below). González et al. (2004) have assigned an age of 10 Myr to L 51 based on the "s" parameter (Elson & Fall 1988), in agreement with our estimate of t = 15 ± 10 Myr (Fig. 11).

3.3.11. K 42

The OGLE database includes a CMD for this cluster (OGLE-CL-SMC0124), with an isochrone based age estimate of 39.8 ± 9.2 Myr (Pietrzynski et al. 1998; Pietrzynski & Udalski 1999). The study by de Oliveira et al. (2000) obtained for it a younger age, 20 ± 10 Myr, which seems too low compared to our estimate, t = 45 ± 15 Myr (Fig. 12).

3.3.12. L 66

The OGLE database includes a CMD for this cluster (OGLE-CL-SMC0129), with an isochrone based age of 20.0 ± 4.6 Myr (Pietrzynski et al. 1998; Pietrzynski & Udalski 1999). This result is comparable to our age estimate of t = 15 ± 10 Myr (Fig. 13).

3.3.13. NGC 411

The spectral features and continuum slope of NGC 411 are comparable to the template spectrum Ia (1 Gyr), when a reddening correction of $E(B-V) = 0.03$ is applied to the observed spectrum (Fig. 14). Although this age estimate is lower than that obtained by Bica et al. (1986), i.e., 3.4 ± 0.3 Gyr (and $[Z/Z_\odot] = -1.3 \pm 0.2$), the present result agrees with the study by Leonardi & Rose (2003) involving integrated spectroscopy at a higher resolution who obtained $t = 1.2 \pm 0.2$ Gyr and [Fe/H] = −0.43 ± 0.14. In addition, two studies involving isochrone fittings to CMDs yield similar results: Da Costa & Mould (1986) obtain t = 1.5 ± 0.5 Gyr and [Fe/H] = −0.9 ± 0.3, adopting a reddening of $E(B-V) = 0.04$ and Alves & Sarajedini (1999) determined t = 1.4 ± 0.2 Gyr and [Fe/H] = −0.68 ± 0.07, based on HST data. By using CCD Washington photometry, a metallicity of [Fe/H] = −0.84, which agrees with the previous, more recent estimates, was derived for this cluster by Piatti et al. (2002b).

3.3.14. NGC 419

An age lower limit of 1 Gyr was obtained for this cluster (OGLE-CL-SMC0159) by isochrone fitting to OGLE data (Pietrzynski et al. 1998; Pietrzynski & Udalski 1999). This age limit is in accord with the other recent age estimates by Rich et al. (2000), who obtained 2.0 ± 0.2 Gyr by means of isochrone fitting to the cluster HST CMD, and by Durand et al. (1984), who estimated 1.2 ± 0.5 Gyr by using isochrone fitting to photographic CMDs. The template matching method yields t = 0.75 Gyr (Fig. 15), but when this value is combined with an independent estimate from the *EW* method, the age converges to 1.2 ± 0.4 Gyr, in close agreement with the result found by Durand et al. (1984). This age is consistent with [Fe/H] = −0.7 (Piatti et al. 2002b).

3.3.15. NGC 422

As far as we know, the only age information on this cluster is based on its integrated colours. González et al. (2004) have considered NGC 422 as a member of the 50 Myr group (SWB type II), which is younger than our estimate of t = 400 Myr (Fig. 16), based on the template method. The final adopted age for NGC 422 is t = 300 ± 100 Myr, which results from the independent methods employed in the present work.

3.3.16. NGC 458

Age determinations of NGC 458 based on isochrone fitting to the cluster CMD were made by Papenhausen & Schommer (1988), Stothers & Chin (1992) and more recently by Alcaino et al. (2003), who obtained 300 Myr, 100 Myr and 140 Myr, respectively. Independent age estimates using the template matching (Fig. 18) and the *EW* methods give t = 50 Myr. Taking into account the previous literature determinations, a final value of $t = 130 \pm 60$ Myr was adopted, which is consistent with [Fe/H] = −0.23 (Piatti et al. 2002b).

4. Discussion

Figure 19 shows the positions of the studied clusters (crossed boxes) relative to the SMC optical centre (cross), assumed to be placed (J2000) at: $00^{h}\ 52^{m}\ 45^{s}$, $-72^{\circ}\ 49'\ 43''$ (Crowl et al. 2001). For the sake of completeness, we included 19 additional clusters (triangles) taken from Table 4 of Piatti et al. (2002b) and studied by Piatti et al. (2005), which have ages and metallicities put onto a homogeneous scale. The collection of these 37 objects constitutes at the present time the largest sample of SMC clusters used to address the issue of the galaxy chemical evolution. Thus, the results derived from this sample are valuable in the sense that they give us the opportunity to have some clues about the galaxy history, which obviously needs later confirmation from a larger database. Besides the SMC Bar, represented by a straight line in Fig. 19, we traced two ellipses centred at the SMC optical centre with their major axes aligned with the galaxy Bar. We adopted a b/a ratio which equals to 1/2. The semi-major axes of the ellipses drawn in the figure have 2° and 4°, respectively. Note that this elliptical geometry matches the space distribution of clusters more properly than a circular one.

When describing the cluster age and metallicity distributions, the interpretation of the results can depend on the spatial framework used. For example, one can adopt as a reference system the one corresponding to the right ascension and declination axes, or that centred on the galaxy with a coordinate axis parallel to the Bar. Thus, if there existed an abundance gradient from the centre and along the SMC Bar, its projection to the right ascension and declination axes would appear steeper. Similarly, it could be possible to affirm the existence of features which are actually the result of projection effects on these directions. By considering the distances of the clusters from the SMC centre instead of their projections onto the right ascension and declination axes, the genuine cluster age and metal abundance variations can be traced. Moreover, although it may be advantageous to plot ages and metallicities as a function of the distance from the galaxy centre, these plottings can result even more meaningful when the spatial variable reflects the flattening of the system. In the case of the SMC, this can be accomplished by using ellipses instead of circles around the SMC centre.

In order to examine how the cluster ages vary in terms of the distances from the SMC centre, we computed for each cluster the value of the semi-major axis (a) that an ellipse would have if it were centred at the SMC centre, had a b/a ratio of 1/2, and one point of its trajectory coincided with the cluster position. Figure 20 shows the result obtained, in which we used the same symbols as in Fig. 19. The figure reveals that there are very few clusters younger than 4 Gyr in the outer disk, defined as the portion of the SMC disk with $a \geq 3.5°$. Conversely, it would appear that there are very few clusters older than 4 Gyr in the inner disk. Furthermore, in the inner disk, the older the clusters, the larger their corresponding semi-major axes, which astonishingly suggests the possibility that the clusters were formed outside in, like in a relatively rapid collapse. As far as we are aware, this is the first time such an evidence is presented.

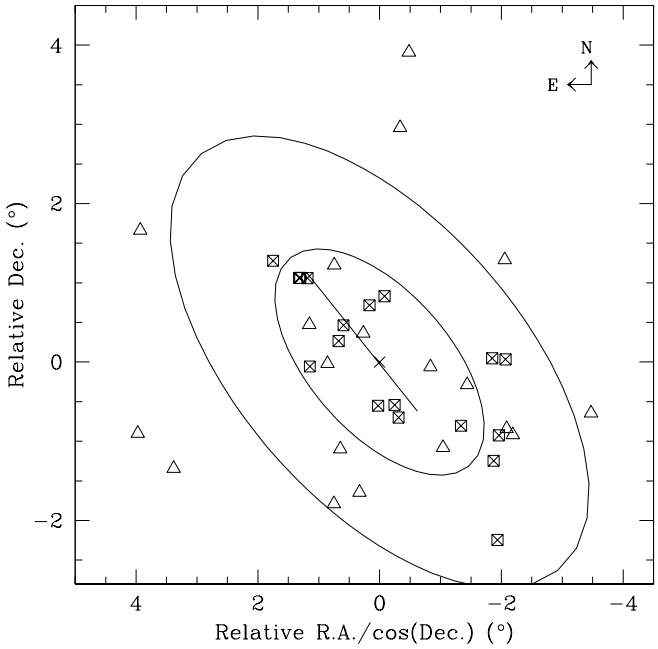

Fig. 19. Positions of the eighteen studied cluster fields (crossed boxes) and of the nineteen additional clusters taken from Piatti et al. (2002b) and Piatti et al. (2005) (triangles) with relation to the SMC bar (straight line) and optical centre (cross). Two ellipses of semi-major axes of 2° and 4° (b/a = 1/2), aligned along the SMC Bar, are also drawn.

Harris & Zaritsky (2004) recently determined the global star formation and chemical enrichment history of the SMC within the inner $4° \times 4.5°$ area of the main body, based on $UBVI$ photometry of ∼6 million stars from their Magellanic Clouds Photometric Survey (Zaritsky et al. 1997). Among other results, they found that there was a rise in the mean star formation rate during the most recent 3 Gyr punctuated by bursts at 2.5 Gyr, 400 Myr, and 60 Myr. The two older events coincide with past perigalactic passages of the SMC around the Milky Way (see, e.g., Lin et al. 1995). In addition, Harris & Zaritsky (2004) derived a chemical enrichment history in agreement with the age-metallicity relation of the SMC clusters and field variable stars. This chemical enrichment history is consistent with the model of Pagel & Tautvaisiene (1999), lending further support to the presence of a long quiescent period ($3 <$ age(Gyr) < 8.4) in the SMC early history. Piatti et al. (2005) confirmed that ∼2.5 Gyr ago the SMC reached the peak of a burst of cluster formation, which corresponds to a very close encounter with the LMC according to recent dynamic models of Bekki et al. (2004). It would seem reasonable, therefore, to accept that the burst which took place 2 Gyr ago formed both clusters and stars simultaneously. Particularly, the 2.5 Gyr star burst appears to have an annular structure and an inward propagation spanning ∼1 Gyr (Harris & Zaritsky 2004).

Piatti et al. (2005) studied 10 clusters mainly located in the southern half of the SMC with ages and metallicities in the ranges 1.5–4 Gyr and $-1.3 <$ [Fe/H] < -0.6, respectively. They also favoured a bursting cluster formation history as opposed to a continuous one for the SMC. The age-position

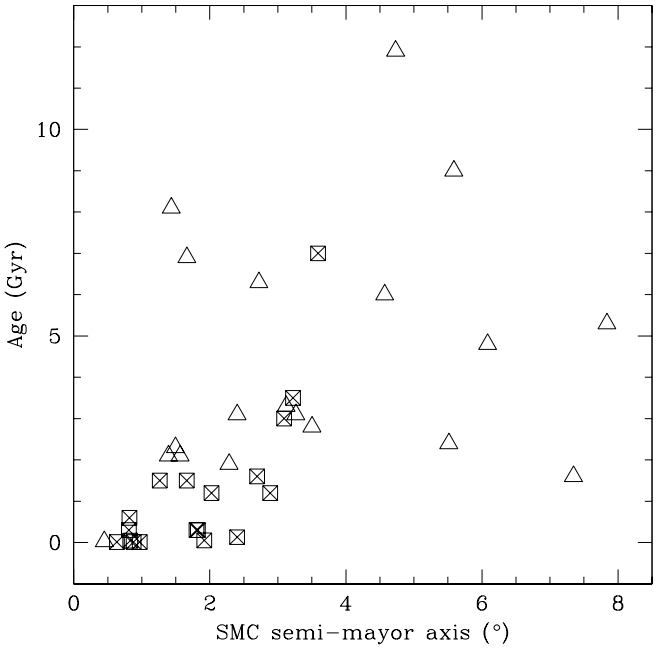

Fig. 20. Cluster ages versus semi-major axes of ellipses with b/a = 1/2, centred at the SMC optical centre, aligned along the SMC Bar, that pass through the cluster positions. Symbols are as in Fig. 19.

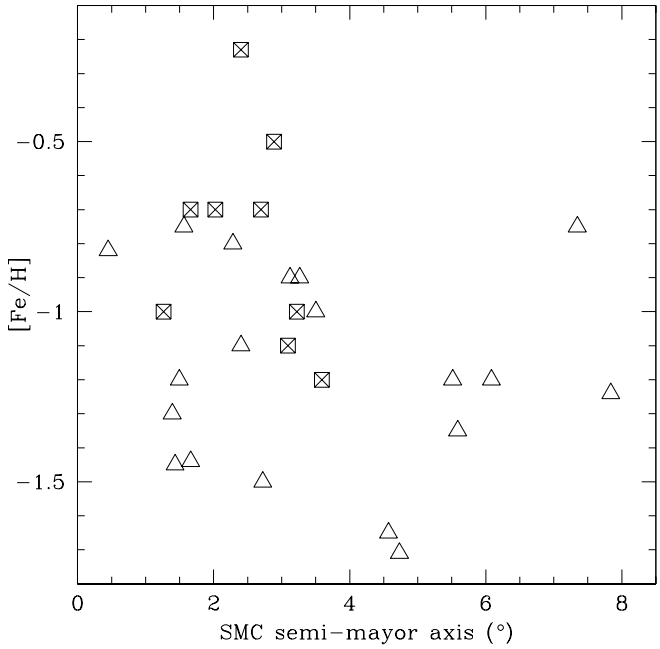

Fig. 21. Cluster metallicity versus semi-major axes of ellipses with b/a = 1/2, centred at the SMC optical centre, aligned along the SMC Bar, that pass through the cluster positions. Symbols are as in Fig. 19.

relation shown in Fig. 20 for clusters younger than 4 Gyr adds, if it is confirmed, a new piece of evidence to the bursting conception of cluster formation. In the case of the cluster formation episode peaking at ∼2.5 Gyr (Piatti et al. 2005), the burst could have triggered the formation process which continued producing clusters from the outermost regions to the innermost ones in the inner SMC disk. On this basis, the inner disk could have been formed during this period.

The distribution of the cluster metal abundances as a function of the distances from the SMC centre is depicted in Fig. 21, where we used the same symbols as in Fig. 19. Note that in the outer disk, there are no clusters with iron-to-hydrogen ratios larger than [Fe/H] = −1.2, with only one exception. On the other hand, the inner disk is shared by both metal-poor and metal-rich clusters, the averaged metallicity being clearly larger than that for the outer disk. We thus confirm the existence of a metal abundance gradient for the SMC disk, in the sense that the farther a cluster from the galaxy centre, the poorer its metal content. However, all the clusters with [Fe/H] > −1.2 in the inner disk were formed during the last 4 Gyr, whereas the metal-poor ones are as old as those in the outer disk (see Fig. 20). Consequently, the abundance gradient seems to reflect the combination between an older and more metal-poor population of clusters spread throughout the SMC and a younger and metal-richer one mainly formed in the inner disk. Note that some few clusters were also formed in the inner disk with [Fe/H] ∼ −1.2 (Fig. 21). We also recall that the present cluster sample follows the age-metallicity relation discussed in a previous work (Piatti et al. 2005, see their Fig. 6).

5. Concluding remarks

As part of a systematic spectroscopic survey of star clusters in the SMC, we present and analise in the current paper flux-calibrated integrated spectra of 18 concentrated star clusters which, with a few exceptions, lie within the inner parts of the SMC. The sample of SMC clusters studied by means of integrated spectroscopy has now been considerably increased. Therefore, the present cluster spectral library at the SMC metallicity level can be useful for future analyses of star clusters in dwarf galaxies as well as for the study of a fraction of star clusters in massive galaxies.

$E(B - V)$ colour excesses were derived for the present cluster sample by interpolation between the extinction maps published by Burstein & Heiles (1982) and by Schlegel et al. (1998). Using template spectra with well determined cluster properties and equivalent widths (*EW*s) of the Balmer and several metallic lines, we determined ages and, in some cases, metallicities as well. For the SMC clusters HW 8 and IC 1641, the ages have been determined for the first time, while for the rest of the studied sample the ages derived from the template matching and *EW* methods exhibit very good agreement. Metal abundances have been derived for five clusters (L 5, K 5, K 3, K 6 and K 28), while we have adopted averaged metallicities from published values for other 4 clusters (K 7, NGC 411, NGC 419 and NGC 458). By combining the present cluster sample with 19 additional SMC clusters with ages and metallicities in a homogeneous scale, we analise the age and metallicity distributions in different regions of the SMC to probe the galaxy chemical enrichment and its spatial distribution. Very few clusters younger than 4 Gyr are found in the outer disk and, conversely, very few clusters older than 4 Gyr lie in the

inner disk. Furthermore, the present age-position relation for the SMC clusters in the inner disk suggests not only the possibility that the clusters were formed outside in, like in a relatively rapid collapse, but also that the inner disk itself could have been formed during a bursting formation mechanism, with an important cluster formation event centred at ∼2.5 Gyr. According to the recent results obtained by Harris & Zaritsky (2004), this cluster burst, which occurred ∼2.5 Gyr ago, is clearly related to an episode of enhanced star formation having taken place about the same time ago. Evidence is also presented on the existence of a radial metal abundance gradient for the SMC disk, which reflects the combination between an older and more metal-poor population of clusters distributed throughout the SMC and a younger and metal-richer one mainly formed in the inner disk.

Acknowledgements. We are grateful for the use of the CCD and data acquisition system at CASLEO, supported under US National Science Foundation (NSF) grant AST-90-15827. This work is based on observations made at CTIO, which is operated by AURA, Inc., under cooperative agreement with the NSF. We thank the staff members and technicians at CASLEO and CTIO for their kind hospitality and assistance during the observing runs. We gratefully acknowledge financial support from the Argentinian institutions CONICET, Agencia Nacional de Promoción Científica y Tecnológica (ANPCyT) and Agencia Córdoba Ciencia. We thank Dr. Munari for sending us the spectrum of SMC 3. This work was also partially supported by the Brazilian institution FAPEMIG and CNPq.

References

Abia, C., & Isern, J. 2000, ApJ, 536, 438
Ahumada, A. V., Clariá, J. J., Bica, E., & Dutra, C. M. 2002, A&A, 393, 855
Alcaino, G., Alvarado, F., Borissova, J., & Kurtev, R. 2003, A&A, 400, 917
Alves, D. R., & Sarajedini, A. 1999, ApJ, 511, 225
Barnbaum, C., Stone, R. P. S., & Keenan, P. C. 1996, ApJS, 105, 419
Bellazzini, M., Ibata, R., Monaco, L., et al. 2005, MNRAS, in press
Bekki, K., Couch, W. J., Beasley, M. A., et al. 2004, ApJ, 610, L93
Bica, E. 1988, A&A, 195, 76
Bica, E., & Alloin, D. 1986, A&A, 162, 21
Bica, E., Dottori, H., & Pastoriza, M. 1986, A&A, 156, 261
Bica, E., & Dutra, C.M. 2000, AJ, 119, 1214
Bica, E., & Schmitt, H. R. 1995, ApJS, 101, 41
Brocato, E., Di Carlo, E., & Menna, G. 2001, A&A, 374, 523
Burstein, D., & Heiles, C. 1982, AJ, 87, 1165
Cioni, M. R., van der Marel, R. P., Loup, C., & Habing, H. J. 2000, A&A, 359, 601
Crowl, H. H., Sarajedini, A., Piatti, A. E., et al. 2001, AJ, 122, 220
Da Costa, G. S. 1991, IAUS, 148, 183
Da Costa, G. S., & Armandroff, T. E. 1995, AJ, 109, 2533
Da Costa, G. S., & Mould, J. R. 1986, ApJ, 305, 214
de Oliveira, M. R., Dutra, C. M., Bica, E., & Dottori, H. 2000, A&AS, 146, 57
Dolphin, A. E., Walker, A. R., Hodge, P. W., et al. 2001, ApJ, 562, 303
Durand, D., Hardy, E., & Melnick, J. 1984, ApJ, 283, 552
Dutra, C. M., Bica, E., Clariá, J. J., Piatti, A. E., & Ahumada, A.V. 2001, A&A, 371, 895
Dutra, C. M., Bica, E., Clariá, J. J., & Piatti, A. E. 1999, MNRAS, 305, 373
Elson, R. A. W., & Fall, S. M. 1988, AJ, 96, 1383
Girardi, L., Bertelli, G., Bressan, A., et al. 2002, A&A, 391, 195
González, R. A., Liu, M. C., & Bruzual, G. A. 2004, ApJ, 611, 270
Harris, J., & Zaritsky, D. 2004, AJ, 127, 1531
Hodge, P. 1988, PASP, 100, 1051
Hodge, P. 1989, ARA&A, 27, 139
Hodge, P. W., & Wright, F. W. 1974, AJ, 79, 858
Kahabka, P. 2004, A&A, 416, 57
Kron, G. E. 1956, PASP, 68, 125
Lauberts, A. 1982, The ESO/Uppsala Survey of the ESO (B) Atlas, European Southern Observatory, Garching bei Munchen
Leonardi, A. J., & Rose, J. A. 2003, AJ, 126, 1811
Lin, D. N. C., Jones, B. F., & Klemola, A. R. 1995, ApJ, 439, 652
Lindsay, E. M. 1958, MNRAS, 118, 172
Matteucci, A., Ripepi, V., Brocato, E., & Castellani, V. 2002, A&A, 387, 861
Mighell, K. J., Sarajedini, A., & French, R. S. 1998, AJ, 116, 2395
Mould, J. R., Jensen, J. B., & Da Costa, G. S. 1992, ApJS, 82, 489
Munari, U., & Zwitter, T. 2002, A&A, 383, 188
Pagel, B. E. J., & Tautvaisiene, G. 1999, Ap&SS, 265, 461
Papenhausen, P., & Schommer, R. A. 1988, in ed. J. Grindlay, & A. G. Davis Philip (Dordrecht: Kluwer Academic Publishers), IAU Symp., 126, 565
Piatti, A. E., Bica, E., Clariá, J. J., Santos Jr., J. F. C., & Ahumada, A. V. 2002a, MNRAS, 335, 233
Piatti, A. E., Santos Jr., J. F. C., Clariá, J. J., et al. 2001, MNRAS, 325, 792
Piatti, A. E., Sarajedini, A., Geisler, D., Bica, E., & Clariá, J. J. 2002b, MNRAS, 329, 556
Piatti, A. E., Sarajedini, A., Geisler, D., Seguel, J., & Clark, D. 2005, MNRAS, 358, 1215
Pietrzynski, G., Udalski, A., Kubiat, M., et al. 1998, Acta Astron., 48, 175
Pietrzynski, G., & Udalski, A. 1999, AcA, 49, 157
Rabin, D. 1982, ApJ, 261, 85
Rich, R. M., Da Costa, G. S., & Mould, J. R. 1984, ApJ, 286, 517
Rich, R. M., Shara, M., Fall, S. M., & Zurek, D. 2000, AJ, 119, 197
Santos Jr., J. F. C., Alloin, D., Bica, E., & Bonatto, C. 2002, in ed. D. Geisler, E. K. Grebel, & D. Minniti (San Francisco: ASP), IAU Symp., 207, 727
Santos Jr., J. F. C., Bica, E., Clariá, J. J., et al. 1995, MNRAS, 276, 1155
Santos Jr., J. F. C., & Piatti, A. E. 2004, A&A, 428, 79 (SP)
Schlegel, D., Finkbeiner, D., & Davis, M. 1998, ApJ, 500, 525
Searle, L., Wilkinson, A., & Bagnuolo, W. G. 1980, ApJ, 239, 803
Silva, D. R., & Cornell, M. E. 1992, ApJS, 81, 865
Stone, R., & Baldwin, J. 1983, MNRAS, 204, 347
Stothers, R. B., & Chin, C. L. 1992, ApJ, 390, 136
Zaritsky, D., Harris, J., & Thompson, I. B. 1997, AJ, 114, 1002

Online Material

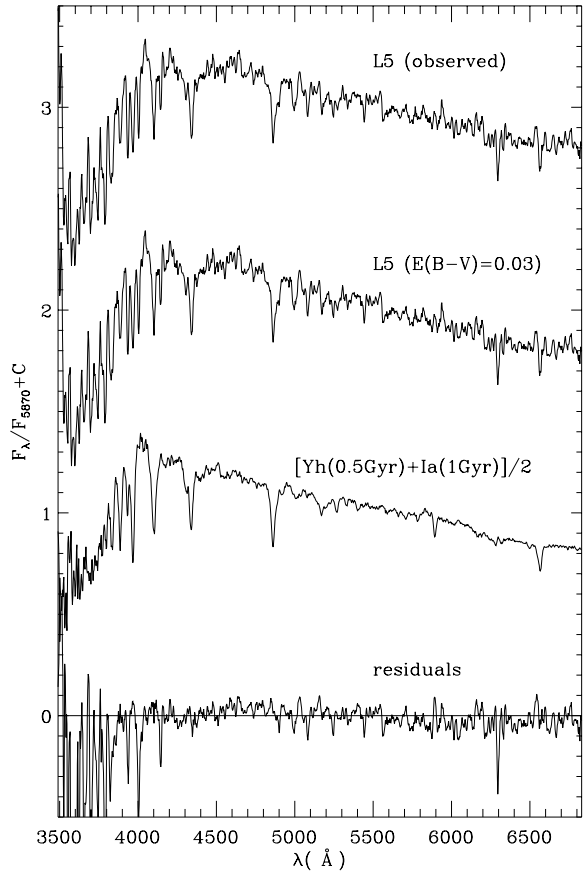

Fig. 1. Observed integrated spectrum of L 5 (*top*), the spectrum corrected for the adopted reddening $E(B-V)$ and the template spectrum which best matches it (*middle*), and the residuals between both (*bottom*). See details in Sect. 3.3.1.

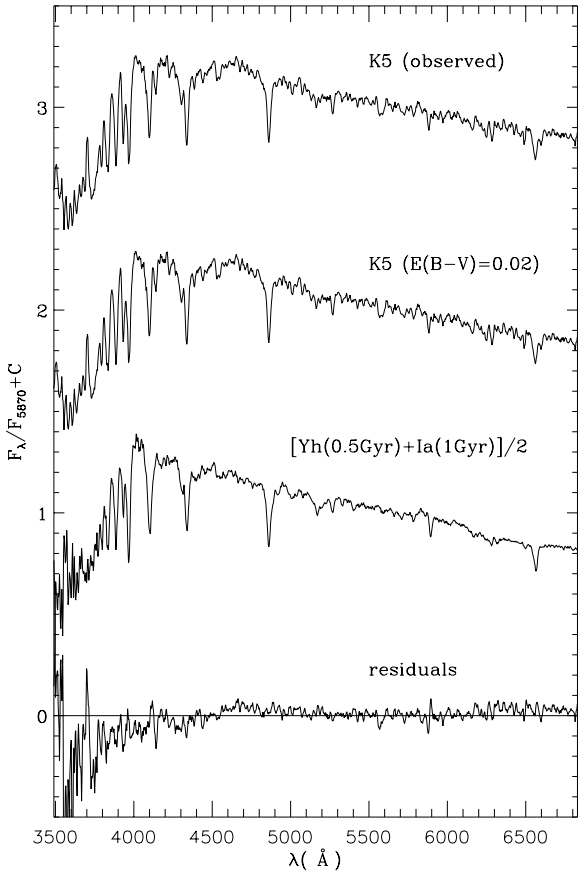

Fig. 2. Observed integrated spectrum of K 5 (*top*), the spectrum corrected for the adopted reddening $E(B-V)$ and the template spectrum which best matches it (*middle*), and the residuals between both (*bottom*). See details in Sect. 3.3.2.

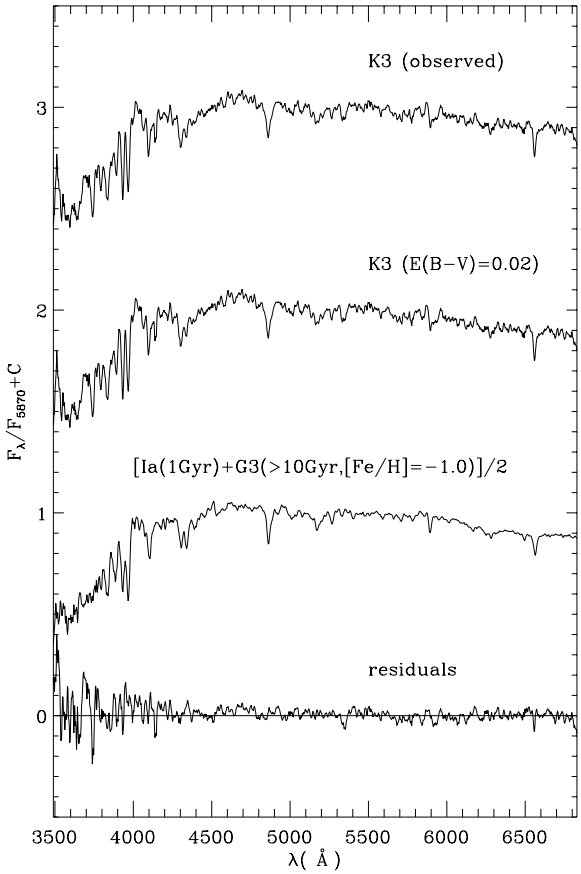

Fig. 3. Observed integrated spectrum of K 3 (*top*), the spectrum corrected for the adopted reddening $E(B-V)$ and the template spectrum which best matches it (*middle*), and the residuals between both (*bottom*). See details in Sect. 3.3.3.

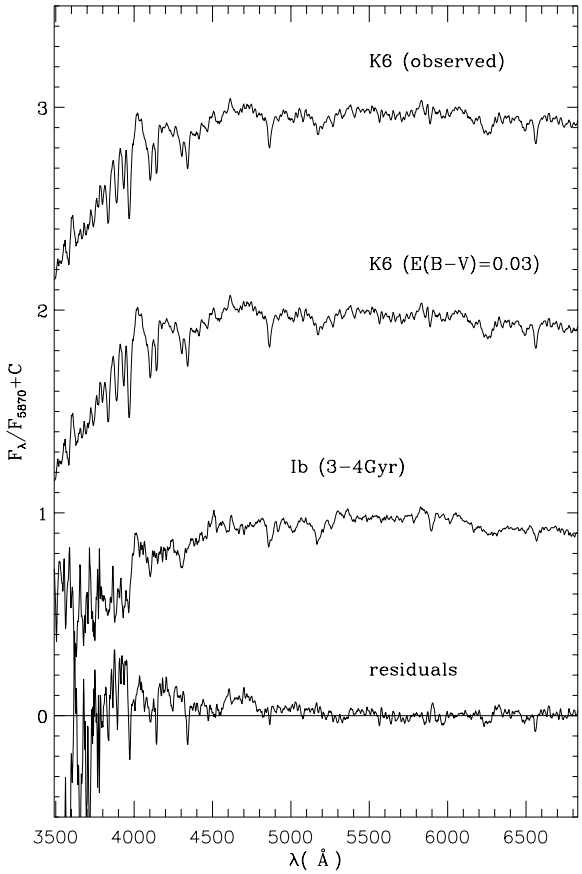

Fig. 4. Observed integrated spectrum of K 6 (*top*), the spectrum corrected for the adopted reddening $E(B-V)$ and the template spectrum which best matches it (*middle*), and the residuals between both (*bottom*). See details in Sect. 3.3.4.

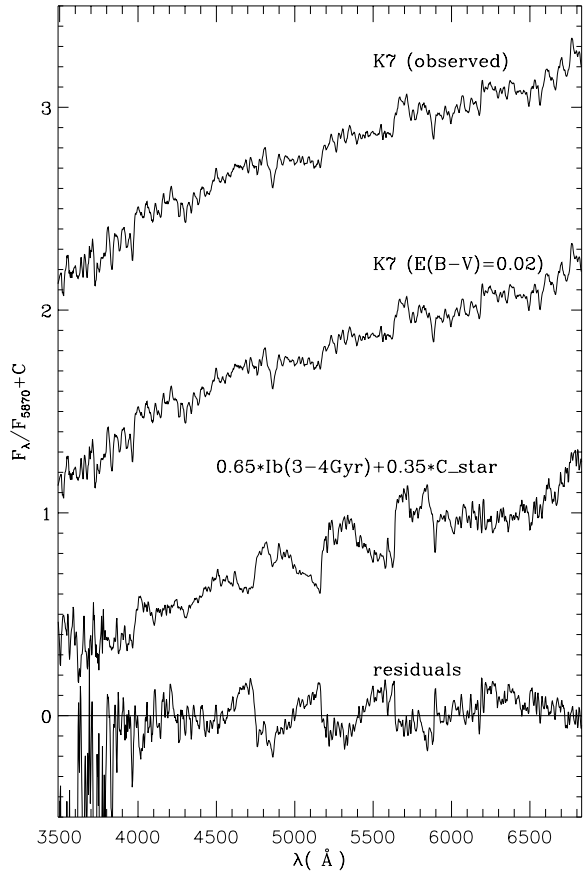

Fig. 5. Observed integrated spectrum of K 7 (*top*), the spectrum corrected for the adopted reddening $E(B-V)$ and the template spectrum which best matches it (*middle*), and the residuals between both (*bottom*). See details in Sect. 3.3.5.

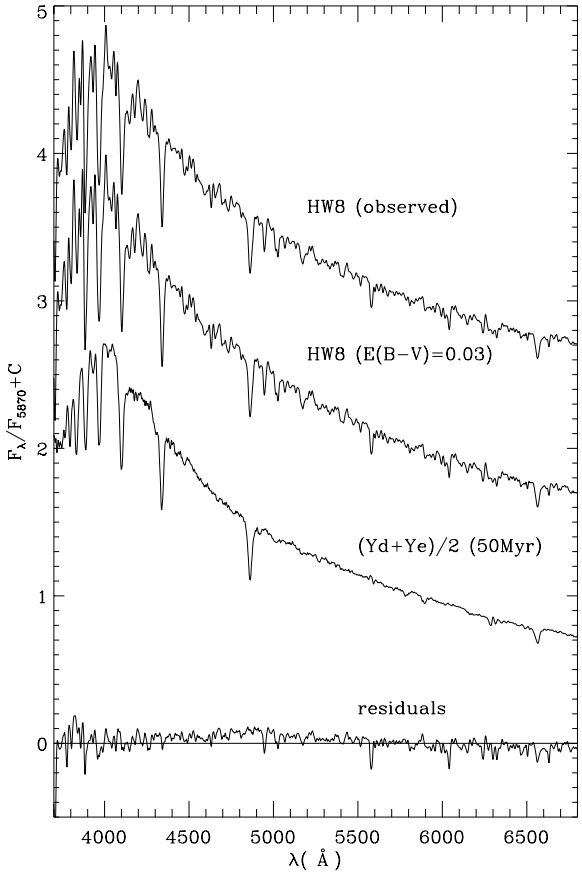

Fig. 6. Observed integrated spectrum of HW 8 (*top*), the spectrum corrected for the adopted reddening $E(B-V)$ and the template spectrum which best matches it (*middle*), and the residuals between both (*bottom*).

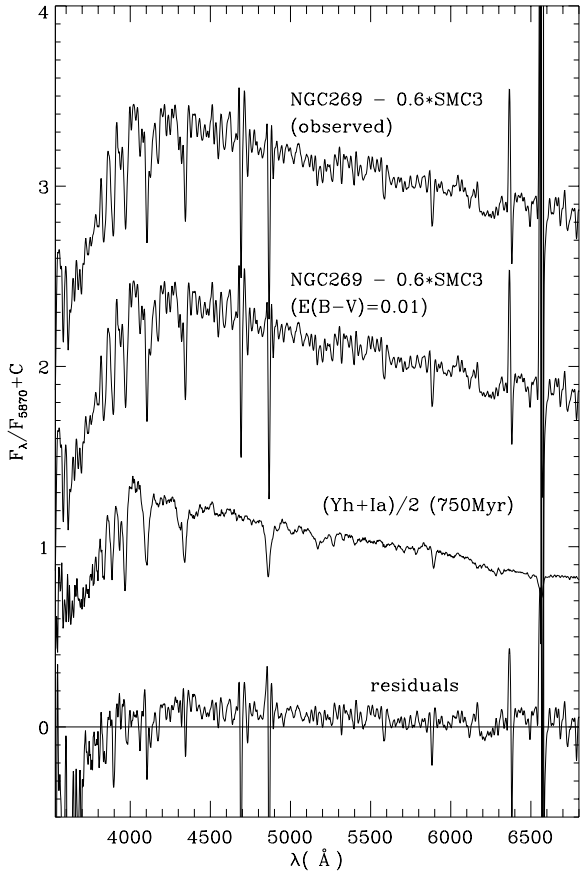

Fig. 7. Observed integrated spectrum of NGC 269 with the symbiotic nova SMC 3 (*top*) subtracted, the spectrum corrected for the adopted reddening $E(B-V)$ and the template spectrum which best matches it (*middle*), and the residuals between both (*bottom*). See details in Sect. 3.3.6.

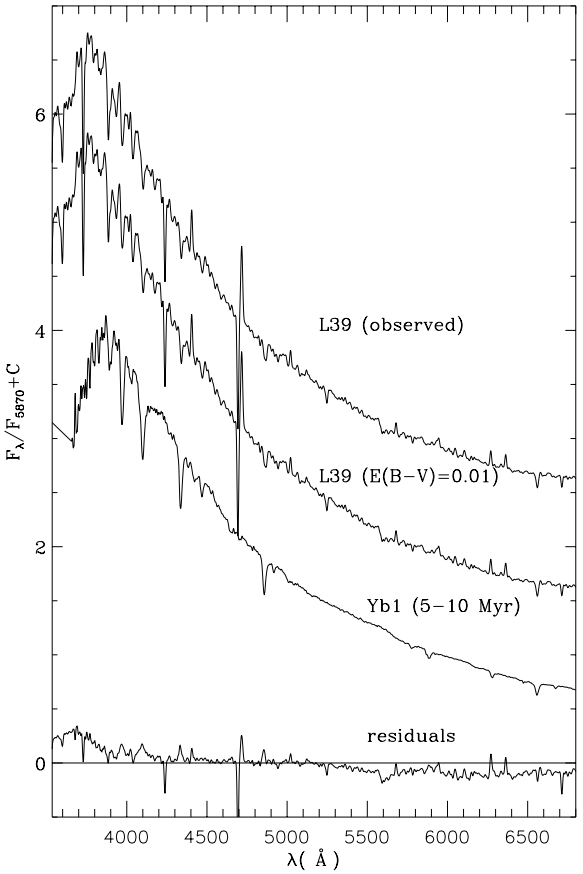

Fig. 8. Observed integrated spectrum of L 39 (*top*), the spectrum corrected for the adopted reddening $E(B-V)$ and the template spectrum which best matches it (*middle*), and the residuals between both (*bottom*). See details in Sect. 3.3.7.

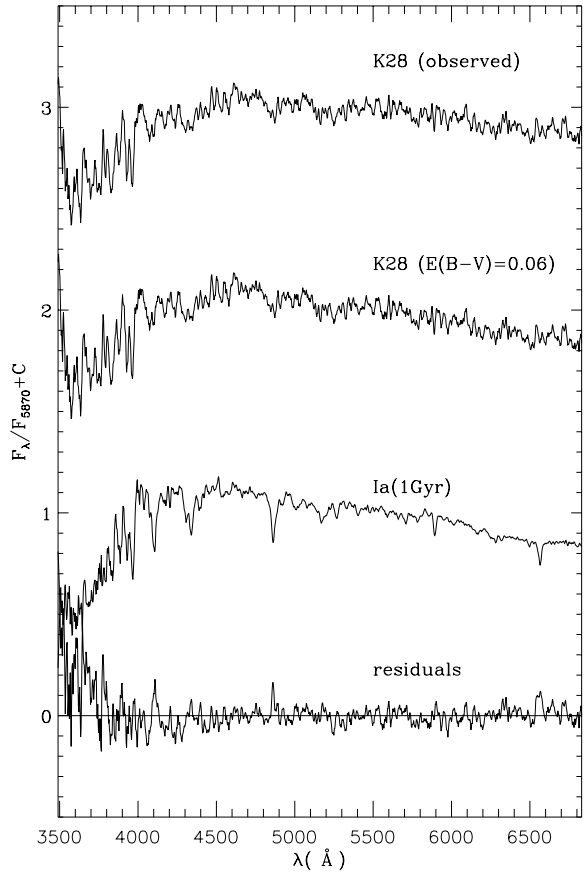

Fig. 9. Observed integrated spectrum of K 28 (*top*), the spectrum corrected for the adopted reddening $E(B-V)$ and the template spectrum which best matches it (*middle*), and the residuals between both (*bottom*). See details in Sect. 3.3.8.

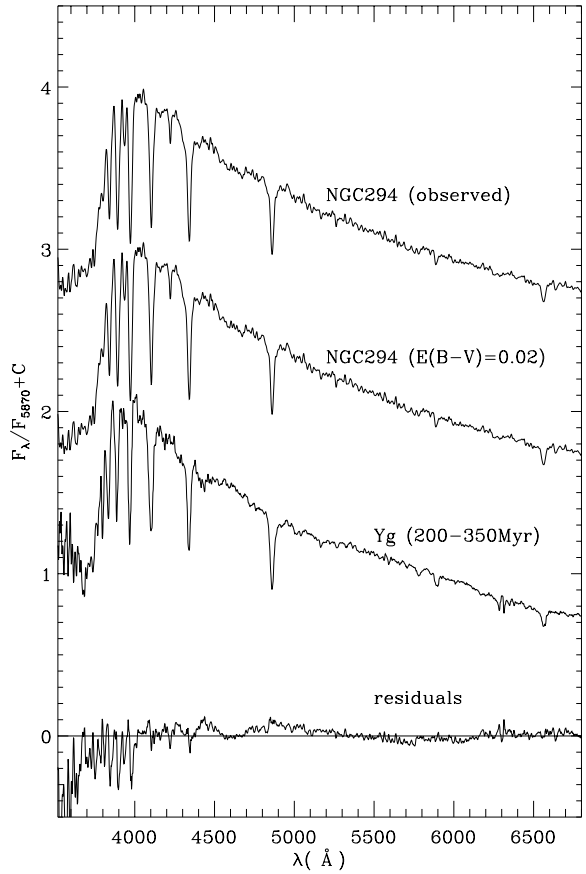

Fig. 10. Observed integrated spectrum of NGC 294 (*top*), the spectrum corrected for the adopted reddening $E(B-V)$ and the template spectrum which best matches it (*middle*), and the residuals between both (*bottom*). See details in Sect. 3.3.9.

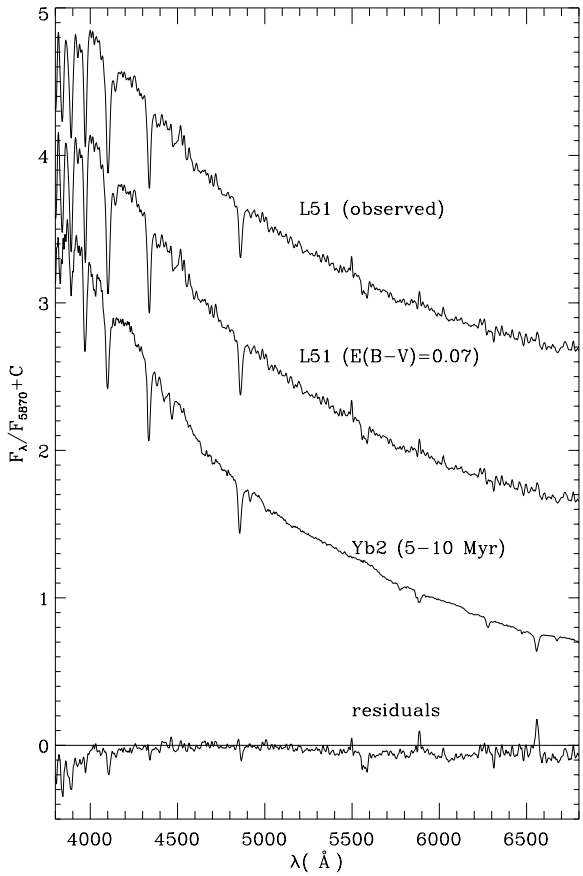

Fig. 11. Observed integrated spectrum of L 51 (*top*), the spectrum corrected for the adopted reddening $E(B-V)$ and the template spectrum which best matches it (*middle*), and the residuals between both (*bottom*). See details in Sect. 3.3.10.

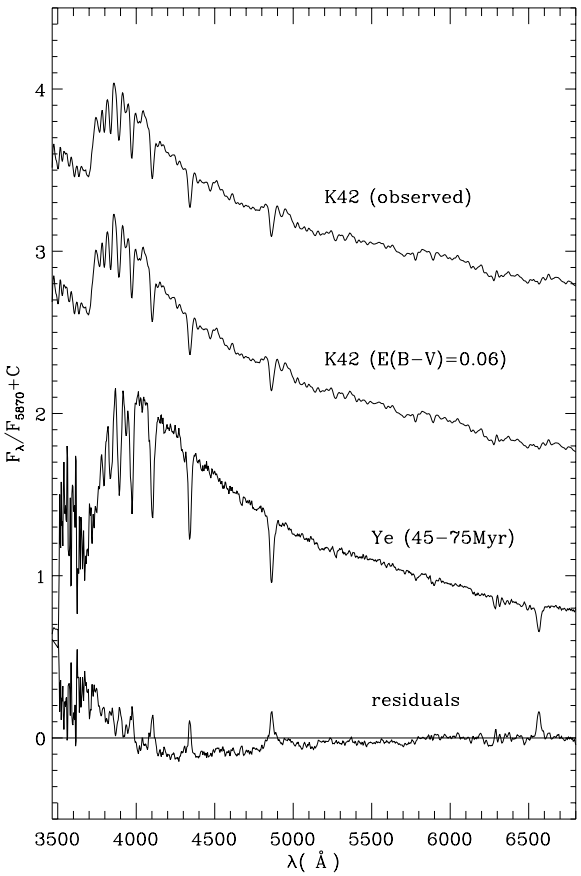

Fig. 12. Observed integrated spectrum of K 42 (*top*), the spectrum corrected for the adopted reddening $E(B-V)$ and the template spectrum which best matches it (*middle*), and the residuals between both (*bottom*). See details in Sect. 3.3.11.

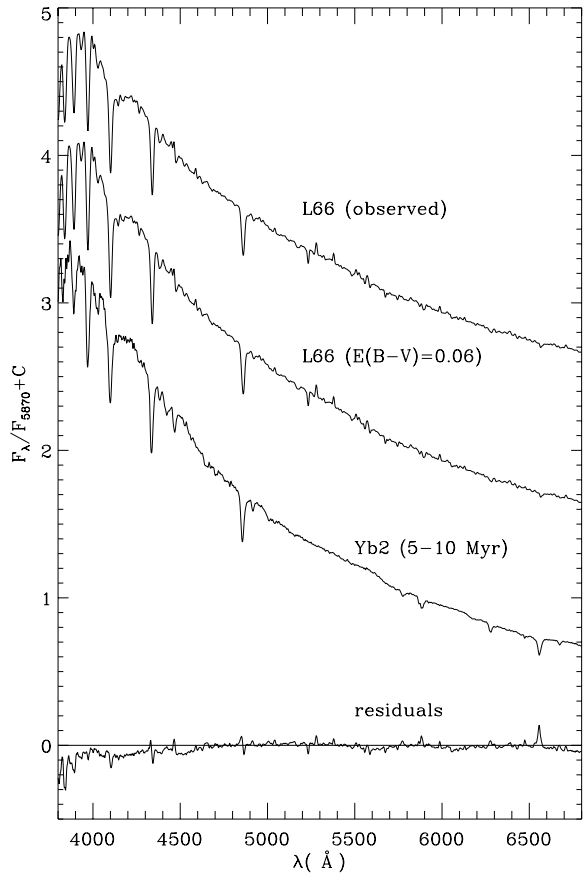

Fig. 13. Observed integrated spectrum of L 66 (*top*), the spectrum corrected for the adopted reddening $E(B-V)$ and the template spectrum which best matches it (*middle*), and the residuals between both (*bottom*). See details in Sect. 3.3.12.

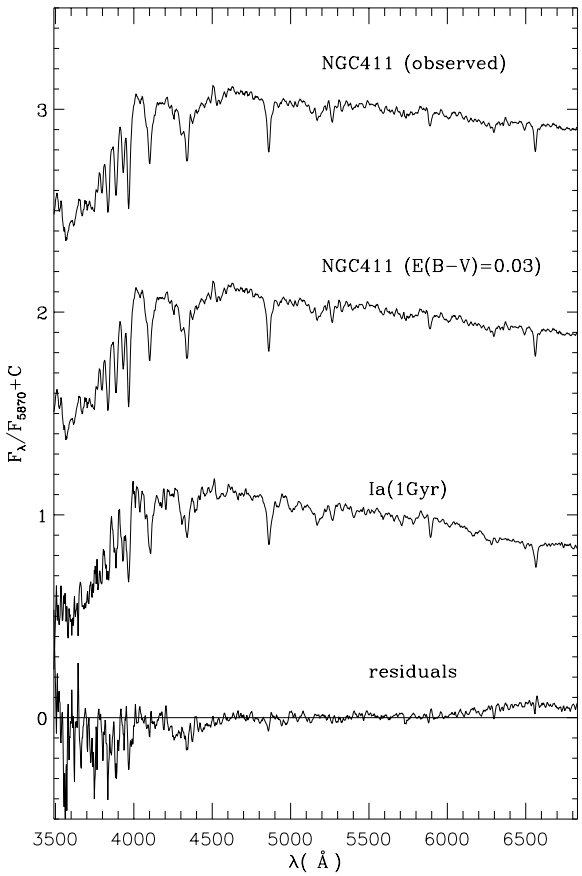

Fig. 14. Observed integrated spectrum of NGC 411 (*top*), the spectrum corrected for the adopted reddening $E(B-V)$ and the template spectrum which best matches it (*middle*), and the residuals between both (*bottom*). See details in Sect. 3.3.13.

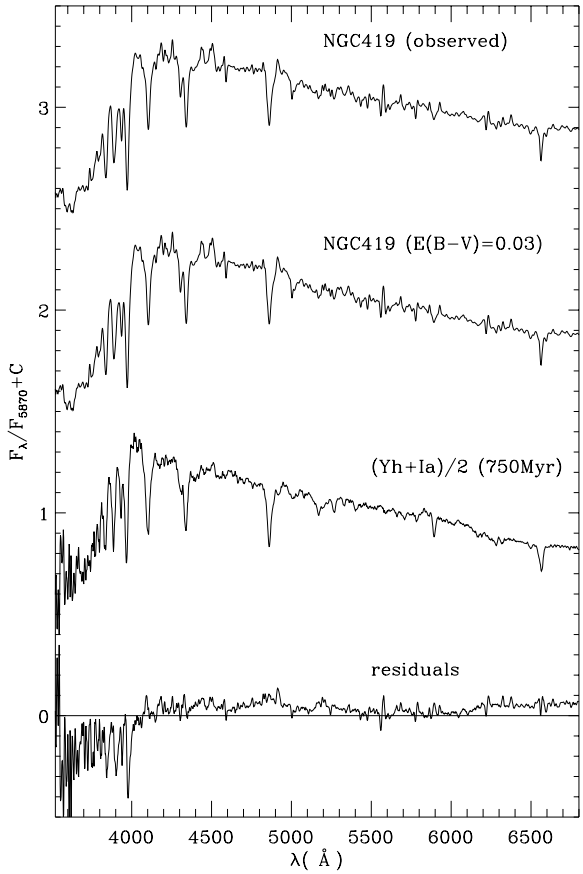

Fig. 15. Observed integrated spectrum of NGC 419 (*top*), the spectrum corrected for the adopted reddening $E(B-V)$ and the template spectrum which best matches it (*middle*), and the residuals between both (*bottom*). See details in Sect. 3.3.14.

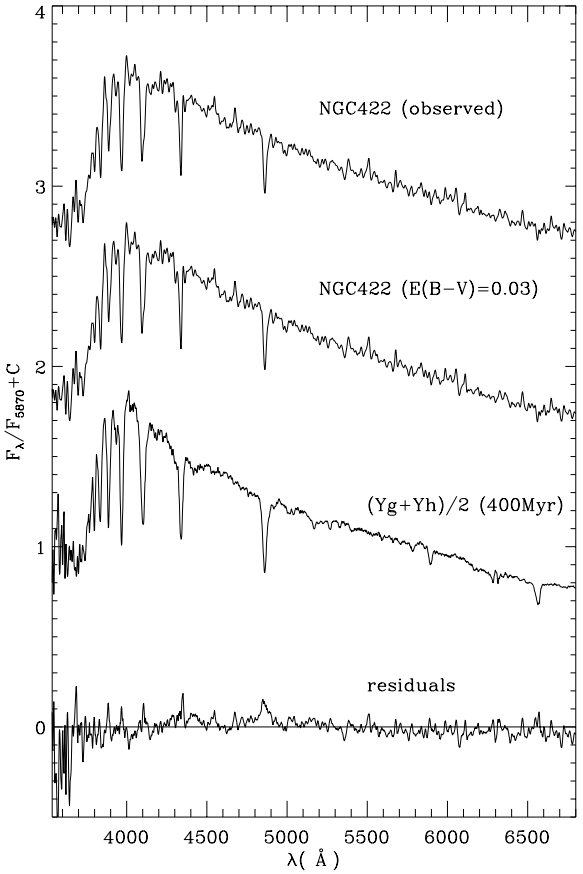

Fig. 16. Observed integrated spectrum of NGC 422 (*top*), the spectrum corrected for the adopted reddening $E(B-V)$ and the template spectrum which best matches it (*middle*), and the residuals between both (*bottom*). See details in Sect. 3.3.15.

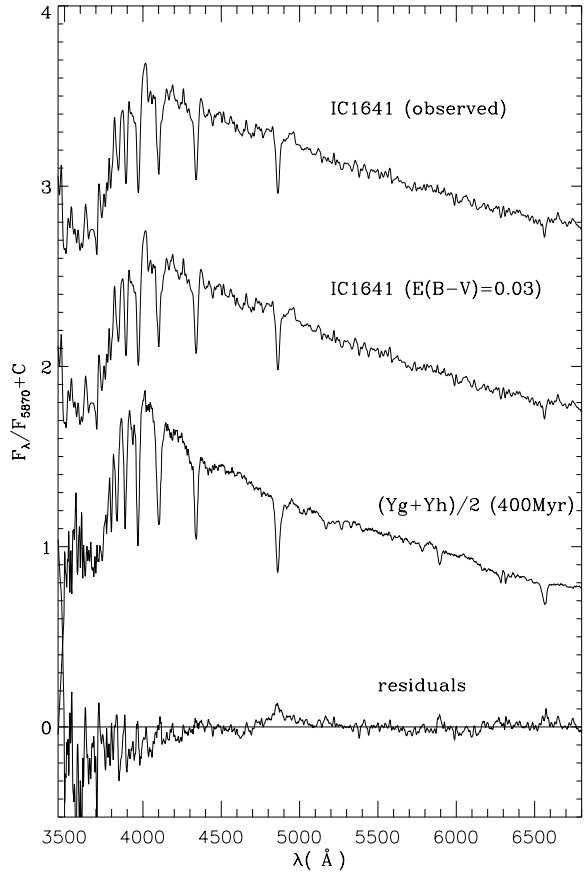

Fig. 17. Observed integrated spectrum of IC 1641 (*top*), the spectrum corrected for the adopted reddening $E(B-V)$ and the template spectrum which best matches it (*middle*), and the residuals between both (*bottom*).

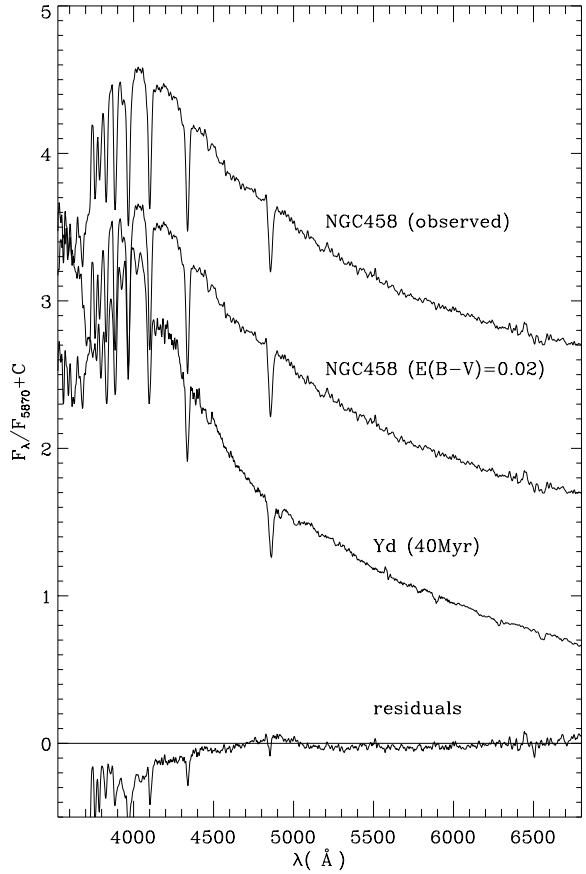

Fig. 18. Observed integrated spectrum of NGC 458 (*top*), the spectrum corrected for the adopted reddening $E(B-V)$ and the template spectrum which best matches it (*middle*), and the residuals between both (*bottom*). See details in Sect. 3.3.16.